INTERNATIONAL JOURNAL OF CLIMATOLOGY
Int. J. Climatol. **25**: 881–894 (2005)
Published online in Wiley InterScience (www.interscience.wiley.com). DOI: 10.1002/joc.1170

A 1° MONTHLY GRIDDED SEA-SURFACE TEMPERATURE DATASET COMPILED FROM ICOADS FROM 1850 TO 2002 AND NORTHERN HEMISPHERE FRONTAL VARIABILITY

SHOSHIRO MINOBE* and ATSUSHI MAEDA
Division of Earth and Planetary Sciences, Graduate School of Science, Hokkaido University, Sapporo, Japan

Received 4 May 2004
Revised 20 November 2004
Accepted 2 December 2004

ABSTRACT

Using surface marine data collected in International Comprehensive Ocean Atmosphere Data Set (ICOADS) release 2.1, a gridded SST dataset on a monthly, $1^\circ \times 1^\circ$ grid is produced from 1850 to 2002. Some unrealistic features, which are commonly found in the gridded SSTs of ICOADS, are removed by a subjective quality control. Based on the gridded SST data, SST variability associated with the oceanic fronts is investigated for the North Atlantic and North Pacific.

Year-to-year SST variability in the North Atlantic is prominent along the climatological Gulf Stream extension (GSE) in winter and spring. This correspondence is captured better in the present SST dataset than in several widely used datasets. GSE mean SST exhibits multidecadal variability similar to the Atlantic multidecadal oscillation represented by mean SSTs over the North Atlantic.

Year-to-year SST variability in the North Pacific in winter and spring seasons is strong along the subarctic front (SAF) and also in the subtropical front (STF), with weaker amplitudes in the latter. In particular, just east of Japan, the Kuroshio extension appears to be a core of strong variability. Winter and spring averaged SAF and STF exhibit prominent decadal warmings in the 1940s, i.e. these fronts may be two of the action centres for the 1940s climate regime shift and the previously reported 1970s shift. The warming anomalies around the SAF associated with the 1940s shift are distributed more broadly than those with the 1970s shift, and have maximal amplitudes around Japan. Copyright © 2005 Royal Meteorological Society.

KEY WORDS: SST; ICOADS; gridded dataset; frontal variability; decadal variability

1. INTRODUCTION

Sea-surface temperature (SST) is a fundamental parameter for discussion of climate variability. SST observations, except for satellite observations, randomly distribute in space and time and are difficult to treat directly. Therefore, tractable gridded SST datasets are quite important for climate research.

In general, SST datasets available through the 20th century can be classified into two categories, i.e. SST datasets with little or no interpolation and heavily interpolated SST datasets. A couple of examples of the former are the UK Meteorological Office historical SST (MOHSST) dataset on a monthly $5^\circ \times 5^\circ$ grid (Parker *et al*., 1995) and gridded SSTs of ICOADS on a monthly $2^\circ \times 2^\circ$ grid. ICOADS (Worley *et al*., 2005) is the successor of the Comprehensive Ocean–Atmosphere Data Set (COADS) (Woodruff *et al*., 1987). Examples of heavily interpolated SST datasets are the Hadley Centre sea ice and sea surface temperature (HadISST) dataset from the UK Met Office (Rayner *et al*., 2003), the Reynolds reconstructed SST data from the National Centers for Environmental Prediction (NCEP; Smith and Reynolds, 2004), and SST data produced by Kaplan *et al*. (1997). These two categories of SST datasets have different advantages and disadvantages. The heavily interpolated SST datasets can have complete spatial and temporal coverage, which is required to

* Correspondence to: Shoshiro Minobe, Division of Earth and Planetary Sciences, Graduate School of Science, Hokkaido University, Sapporo, 060-0810, Japan; e-mail: minobe@ep.sci.hokudai.ac.jp

force atmospheric climate models for studies of climate variability and predictability, and to assess the SST climatology of coupled climate models. The interpolation, however, can include false gridded values. The SST datasets without interpolations do not involve artificial data, but have substantial areas of missing data, especially in the 19th and the early 20th centuries. For recent decades, satellite observations allow global coverage of SST datasets without heavy reliance on interpolations (e.g. Reynolds and Smith, 1994).

In this paper we produce a gridded SST anomaly dataset on a monthly $1^\circ \times 1^\circ$ grid without any spatial smoothing or spatial interpolation of the anomaly field; this dataset has the highest effective resolution compared with the aforementioned SST datasets. As an application of this SST dataset, we analyse the variability of the Gulf Stream extension (GSE) in the North Atlantic, and the subarctic front (SAF) and subtropical front (STF) in the North Pacific.

The rest of the paper is organized as follows. In Section 2 the method of gridding is described. In Section 3 the overall features of global SST fields are explained. The GSE variability is described in Section 4, and the variability of SAF and STF is examined in Section 5. A summary and discussion are presented in Section 6.

2. OBSERVATIONAL DATA AND GRIDDING METHOD

The SST observations used for this dataset were taken from ICOADS release 2.1 (Worley *et al*., 2005). ICOADS includes recent digitalization of the Japanese Kobe Collection for the observations before 1931, and the data coverage has been substantially improved mainly in the Pacific Ocean (Manabe, 1999). Also, Ishii *et al*. (2005) produced a monthly $1^\circ \times 1^\circ$ SST anomaly dataset using ICOADS (release 2.0) and the Kobe Collection. They employed an optimal interpolation technique and also interpolations based on empirical orthogonal functions (EOFs), and hence their dataset is heavily interpolated.

We gridded global SST observations from 1850 to 2002. As will be explained below, some erroneous data were removed by a subjective quality control. The data that passed the subjective assessments were processed for objective quality control and gridding.

2.1. Subjective quality control

Widely used objective quality controls based on a standard deviation of anomalies may be insufficient to remove unrealistic data when the population ratio of the unrealistic data is large in a certain region. An example of an unrealistic feature is a couple of grids of the SST anomalies over the central North Pacific apparent in the gridded version of ICOADS available since 1960 on a $1^\circ \times 1^\circ$ grid (Figure 1). We obtain a similar feature when we produce the SST dataset without a subjective quality control. The problem of

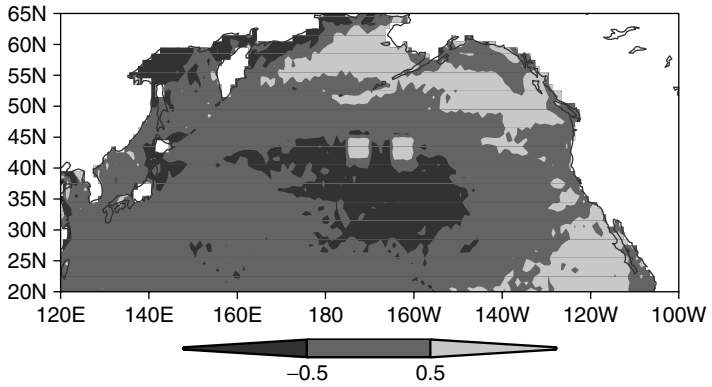

Figure 1. SST difference between 1977–97 and 1960–76 based on gridded ICOADS SSTs on $1^\circ \times 1^\circ$ grid. The SST difference is consistent with the PDO pattern shown by Mantua *et al*. (1997), except for the couple of unrealistic squares (40–45 °N, 175–170 °W and 165–160 °W) in the central North Pacific

unrealistic SSTs over the central North Pacific in ICOADS was known by some researchers (Dr T. Mitchell, personal communication), but the source of the problematic data was not previously documented.

In order to identify the possible sources of the unrealistic SSTs at specific locations and times, we plotted a histogram, a temperature–time scattered diagram, and several other kinds of plots for each of major deck numbers. A deck number is a code number that indicates the source country and organization that obtained the data. From a visual inspection of these plots, we determine how to remove the data that might be the source of the unrealistic feature of the gridded data.

In order to illustrate how we determine the removal scheme, we plot a histogram of the SST data for deck number 732 and SST data for other deck numbers for the aforementioned unrealistic squares over the central North Pacific (40–45 °N, 175–170 °W and 165–160 °W) (Figure 2). Deck number 732 is Russian marine meteorological dataset received at the National Center for Atmospheric Research (NCAR). It is apparent that the probability distribution function for deck number 732 is significantly different from that for other deck numbers. The SSTs of deck number 732 are generally colder than the SSTs of other deck numbers. The number of SST observations of deck number 732 is the largest (40%) in this region, with the second largest observation number of 14%; the ratio of the deck number 732 is too large to be removed by an objective quality control. We suspect that the location of a substantial portion of observations with deck number 732 may be wrong, because the vestige of a similar unrealistic feature is also seen in sea-level pressures (SLPs). The doubtful distribution of deck number 732 is observed only before 1975, and the data after 1976 are likely to be normal.

We also found several other unrealistic observations, and removed them. Observations removed by the subjective quality control are summarized in Table I. Some data listed here can be removed by an objective quality control, but we conservatively removed these apparently unrealistic data subjectively before the objective quality control. The present crude scheme of detection and removal of doubtful observations is useful for the purpose of this study, in which only SST data are gridded. However, it may be insufficient for

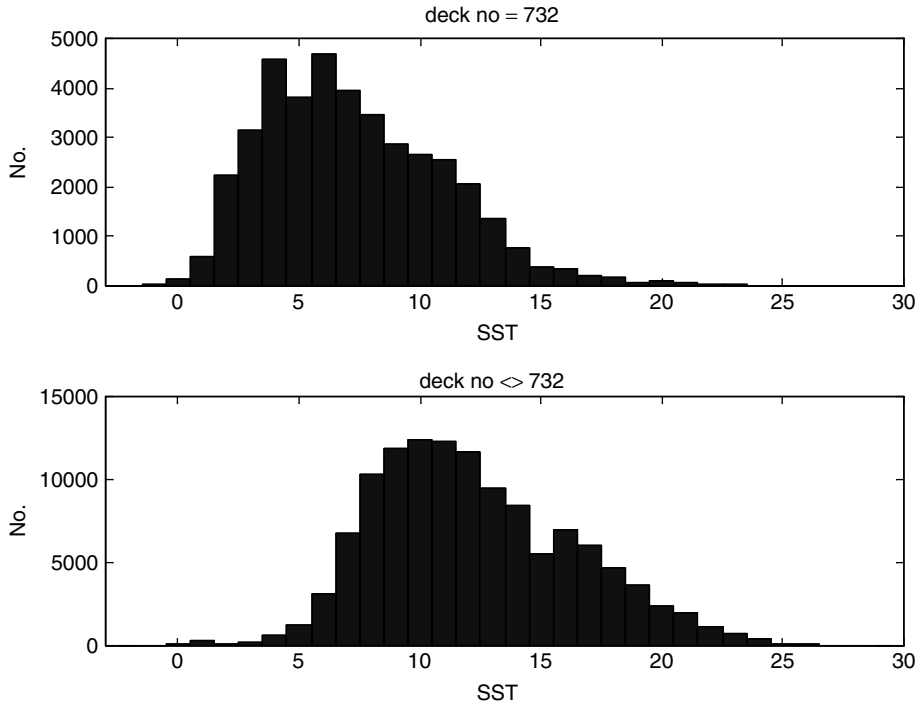

Figure 2. Histogram of SST data of deck number 732 (upper panel) and SST data of other deck numbers (lower panel) over 40–45 °N, 175–170 °W and 165–160 °W. The period is 1956–76 for deck number 732 and 1900–76 for other deck numbers. There is no observation before 1956 for deck number 732 in this region

Table I. Subjectively removed SST data. The last row indicates that the non-bucket observations (engine intake or unknown) of deck numbers 705, 706, and 707 were removed

Region	Lat.	Lon.	Year	SST	Deck no.
Central North Pacific	40–45 °N	175–170 °W and 165–160 °W	1850–1975	All	732
Eastern North Pacific	26–30 °N	125–119 °W	19–1975	All	732
Tropics	20 °S–20 °N	All	All	<3	All
Tropics	20 °S–20 °N	All	All	<5.5	555, 706, 714, 732, 883, 888, 889, 892, 926, 927
Western tropical South Pacific	20 °S–0°	140 °E–175 °W	All	<10	714, 732, 888, 892, 926
East of Madagascar	30–20 °S	50–60 °E	All	<5.0	All
Eastern tropical South Pacific	25–10 °S	100–80 °W	All	<5.5	All
East of southern South America	50–40 °S	60–50 °W	All	All	732
West of southern South America	33–30 °S	10–15 °E	All	All	732
Global	All	All	1939–41	Non-bucket	705, 706, 707

a more general use. In future, it is desirable to detect doubtful data objectively by using a statistical approach, such as a statistical test of difference of distributions between two groups (e.g. different deck numbers).

2.2. *Objective quality control and gridding*

The objective quality control and gridding were conducted as follows. First, we removed the data that are colder than −2 °C or warmer than 37 °C, and the data over land. We temporally calculated the SST climatology for every 5 days on a $1^\circ \times 1^\circ$ grid for the period 1950–2000. (We also examined the quality control using climatology before 1950 and after that, but the major conclusions of the present paper unchanged.) When a monthly climatology value deviates from the annual mean climatology by more than three standard deviations, the monthly climatology was replaced by the missing value. The climatology was further smoothed by a five-point median smoother temporally and zonally. We used these smoothings, because erroneous climatology can yield false anomalies associated with the spatial and temporal changes of observation locations. Since the grid interval for data for which smoothing was applied is high spatially (1°) and temporally (5 days), this moderate smoothing does not obscure major frontal structures as described below. We used the 51 year long base period for calculating climatology in order to suppress noises in the estimated climatology.

The resultant 5 day climatology is interpolated to a 1 day interval using the first four components of sinusoidal functions (annual, semiannual, 4 month, and 3 month components). Anomalies of the respective observations were calculated using bilinear spatial interpolation of daily climatology. Anomalies that had a larger amplitude than 2.5 standard deviations of the anomalies at each grid and month were removed from further analyses. Then, the calculation of climatology and the quality control for the anomalies were repeated. The quality-controlled anomalies were gridded by using simple averaging in a monthly $1^\circ \times 1^\circ$ bin. Neither spatial interpolation nor spatial smoothing is applied to the anomaly field.

The bucket correction of Folland and Parker (1995) was applied to the gridded SST anomalies by interpolating their $5^\circ \times 5^\circ$ correction values onto the $1^\circ \times 1^\circ$ grid. Their correction method assumes that before 1941 all SSTs were measured by buckets. However, recently added SST data for deck numbers 705, 706 and 707 have 80% of SST data measured via engine intake. Thus, for consistency, we also removed these data subjectively before the objective quality control (Table I). We compared the corrected SST anomalies

with the SST data of the World Ocean Database 2001 for the data-rich region around Japan, where correction values are the largest, and did not find any substantial differences. The SST dataset produced in this study consists of the corrected SST anomalies.

3. OVERALL FEATURES OF SST ANOMALIES

Figure 3 shows a comparison of globally averaged monthly temperature anomalies of the present SST, HadiSST, and MOHSST between 60 °S and 70 °N during the period 1880–2002. Overall features, such as warming in the early 20th century and after 1970, are common in all datasets with comparable magnitude. A notable difference is strong cold anomalies from 1939 to 1941 in the present SST, which are not found in either the HadiSST or the MOHSST datasets. To identify the sources of the difference further investigations are required.

Figure 4 shows standard deviations of monthly 1° × 1° SST anomalies during the 20th century. The standard deviations at mid and high latitudes are strong along the oceanic fronts, such as the GSE in the North Atlantic

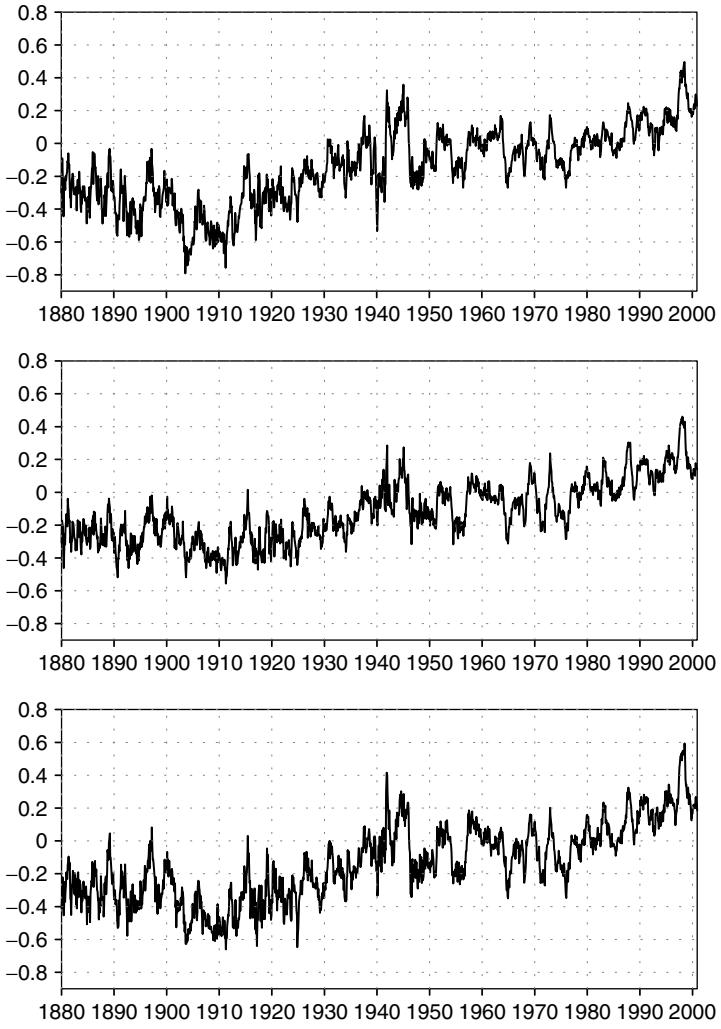

Figure 3. Global average of monthly SST anomalies relative to 1960–90 climatology using the present SST (top), HadiSST (middle), and MOHSST (bottom)

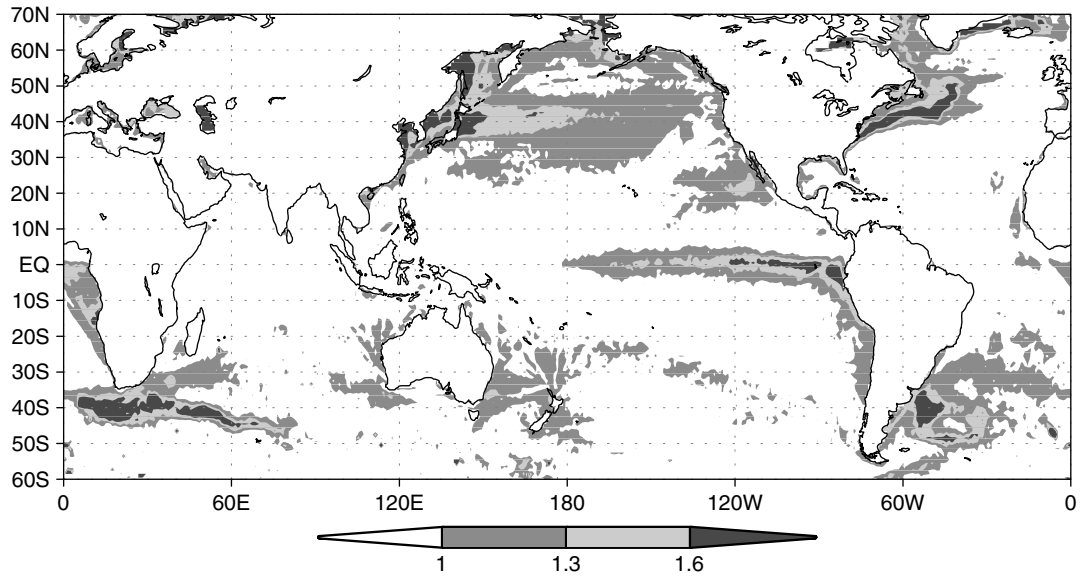

Figure 4. Standard deviation of monthly SST anomalies during the 20th century (1901–2000). The grey-scale bar shows shading convention in units of degrees Celsius

and SAF (around 40 °N) in the North Pacific. Also, strong standard deviations south of Africa and east of South America are associated with climatological frontal structures. The SST variability over the North Atlantic and the North Pacific will be examined more closely in the following sections.

4. GULF STREAM EXTENSION

The strong standard deviation along the GSE in the North Atlantic is worth examining further. The GSE corresponded to the amplitude maxima of the first mode of SSTs in the North Atlantic (Deser and Blackmon, 1993). Moreover, whether the GSE variability significantly influences the atmosphere (Ratcliffe and Murray, 1970; Palmer and Sun, 1985; Joyce *et al*., 2000; Wu and Rodwell, 2003) or not (Frankignoul *et al*., 2001) is an interesting question with respect to the air–sea interaction in the North Atlantic.

Maps of standard deviations in each month indicate that the variability is stronger from December to May, but weaker from June to November (not shown). Winter–spring (December to May) averaged SST anomalies indicate strong variability along the climatological mean SST gradient corresponding to the mean GSE (Figure 5). We also examined the standard deviation map of detrended data for winter–spring SSTs, but the differences in standard deviation between the raw and detrended data are quite small; the pattern correlation is 0.98 and the domain-mean standard deviations for the detrended data are smaller only by 3.4% than that for the raw data.

In figure 6 we compare the standard deviations of winter–spring mean SST anomalies of other widely used long-term SST datasets, i.e. HadISST, ICOADS, and MOHSST, whose spatial grid intervals are 1°, 2° and 5° respectively. For consistency, we applied the bucket SST correction of Folland and Parker (1995) to the ICOADS SSTs. The other two SST datasets were already corrected by the original providers. The present SST dataset depicts more strongly GSE-trapped SST variability than any of the other datasets. HadISST is likely to underestimate the SST variability, and the GSE-related high variability is somewhat broadened. The reason for the underestimation is that a smoothing was applied throughout the dataset, and the intrinsic resolution is lower before 1949 (Dr C. K. Folland, personal communication). Amplitudes in ICOADS are nearly as strong as the present product, but strong variability along the GSE is less well separated from coastal variability.

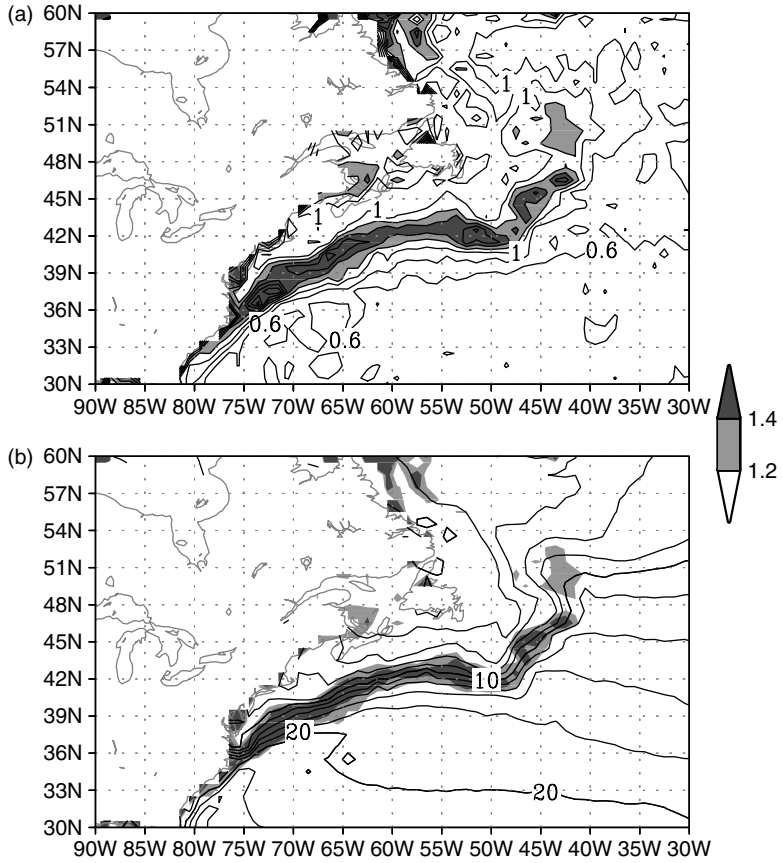

Figure 5. (a) Standard deviation of SST anomalies averaged over December–May (winter–spring) during the 20th century using the present SST data. Contour interval is 0.2 °C with thick contours of 1 °C and 2 °C, and grey-scale bar shows the shading convention. The SST anomalies at grids where standard deviations are larger than 1.3 °C to the east of 75 °W south of 48 °N, except for coastal grids, are used for calculation of the time series of GSE mean SST anomaly shown in Figure 6. (b) Climatological SSTs for December–May with the same shading of the standard deviations as in (a)

The 5° grid interval of MOHSST is apparently too coarse to distinguish the coastal variability and GSE variability. Consequently, the present SST product seems to capture the year-to-year GSE variability during the 20th century most successfully.

We calculate the averaged winter–spring mean SST over grids whose standard deviation is larger than 1.3 °C to the east of 75 °W and south of 48 °N ignoring coastal grids, and call it GSE mean SST (see Figure 5 for which grids are used). The GSE mean SST indicates prominent multidecadal variability in addition to interannual variability (Figure 7). This suggests that the GSE shifted its position on a multidecadal time scale, because the dominant variability of the year-to-year GSE is a lateral shift (Joyce *et al*., 2000; Frankignoul *et al*., 2001). The multidecadal variability is generally consistent with the leading EOF mode of North Atlantic SSTs by Deser and Blackmon (1993). Recently, the dominant multidecadal variability over the North Atlantic has sometimes been called the Atlantic multidecadal oscillation (AMO; Enfield *et al*., 2001). Enfield *et al*. (2001) defined an AMO index as a time series of area-averaged SST anomaly over the North Atlantic. The AMO-like pattern was also shown by Folland *et al*. (1986), who reported that this SST pattern is closely related to decadal variations in Sahel rainfall. Figure 7 also shows the winter–spring AMO time series based on the present SST dataset, indicating the close linkage between the AMO and GSE SST. Actually, if we calculate regression coefficients of SSTs onto the AMO index, the highest regressions are observed along the GSE (not shown).

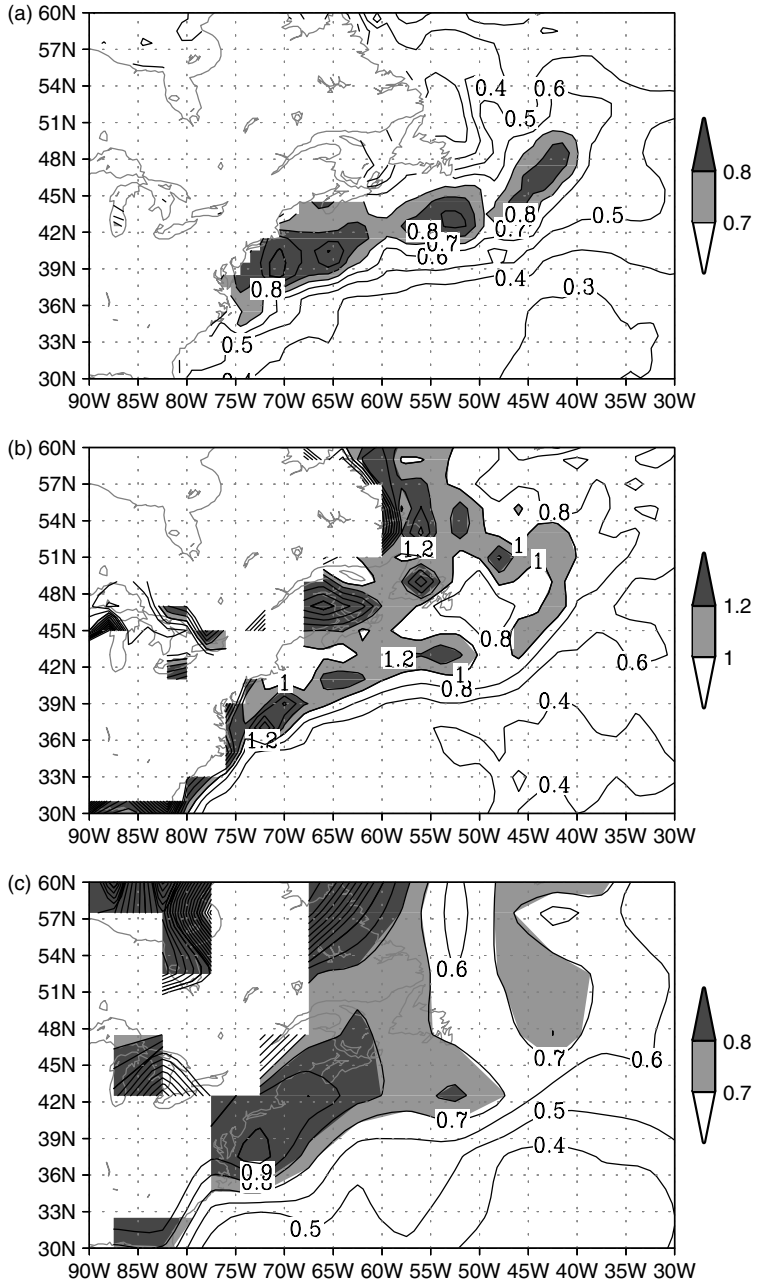

Figure 6. Same as Figure 5(a), but for (a) HadISST (1° × 1° grid), (b) ICOADS SST (2° × 2° grid), and (c) MOHSST (5° × 5° grid). The contour intervals are 0.1 °C for (a) and (c), but 0.2 °C for (b). Shading convention is shown by the grey-scale bars

5. SUB-ARCTIC AND SUB-TROPICAL FRONTS IN THE NORTH PACIFIC

In parallel with the analysis of the North Atlantic, we calculated the standard deviation of SST anomalies averaged over the winter and spring seasons combined (December–May) for the North Pacific (Figure 8). To the east of Japan, it is evident that strong standard deviations have two cores along the Kuroshio extension (KE; 35 °N) and Oyashio front (OF; 40 °N). Also, around 40 °N, 170 °E, another cluster of strong standard deviation is observed. Around this location the northern branch of the Kuroshio bifurcation front merges

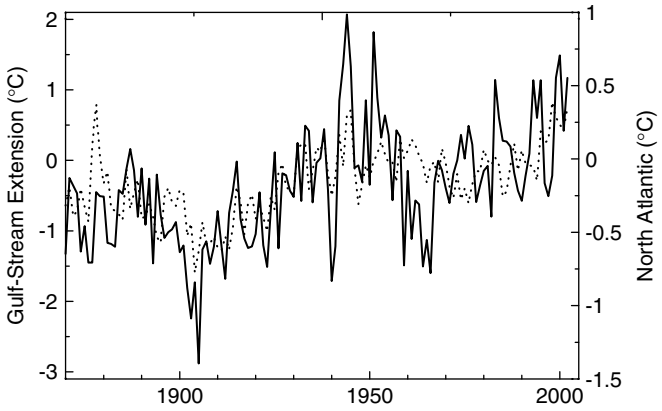

Figure 7. Winter–spring (December–May) averaged GSE SST anomalies (solid line, left axis) along with the North Atlantic mean SST anomalies (dashed line, right axis). Without any smoothing, multidecadal variability is prominent

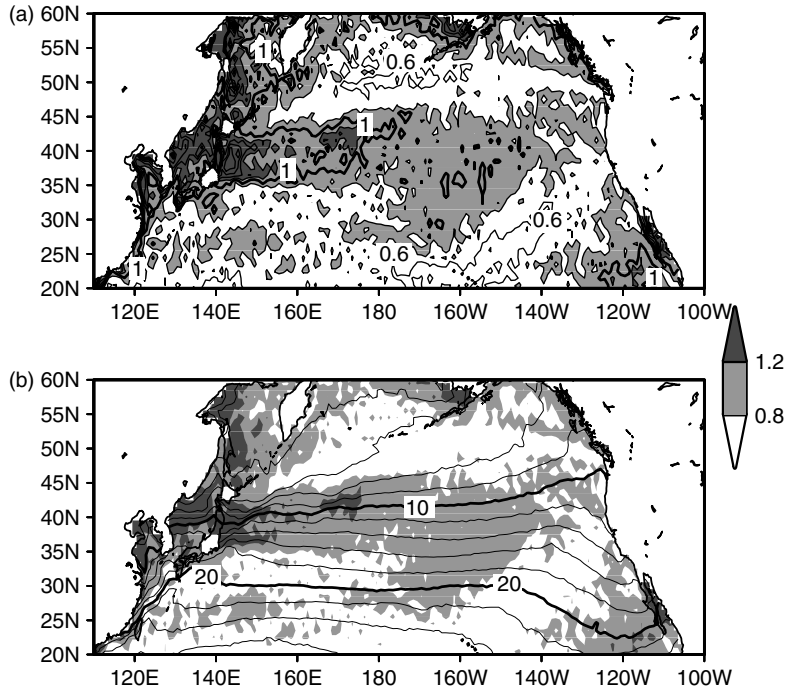

Figure 8. Same as Figure 5, but for the North Pacific

with the OF (Mizuno and White, 1983). Combined with these systems, a broad band of strong mean SST gradients accompanied by large standard deviations around 40 °N is called the SAF (Nakamura *et al*., 1997) or Kuroshio–Oyashio extension (Seager *et al*., 2001; Schneider *et al*., 2002) in climate research. Weaker, but sizable, standard deviations associated with the STF are observed from 25–35°N to the east of the dateline (180–140 °W) and at around 25°N to the west of it.

Figure 9 shows the standard deviation of winter–spring SST anomalies based on the other SST datasets. Again, detailed spatial structures, i.e. two cores associated with the KE and OF, are smoothed out in HadiSST and MOHSST. The two-core structure is barely captured by the ICOADS, but the other maximum at around the merging region of the OF and the northern branch of the Kuroshio bifurcation front is absent. In addition,

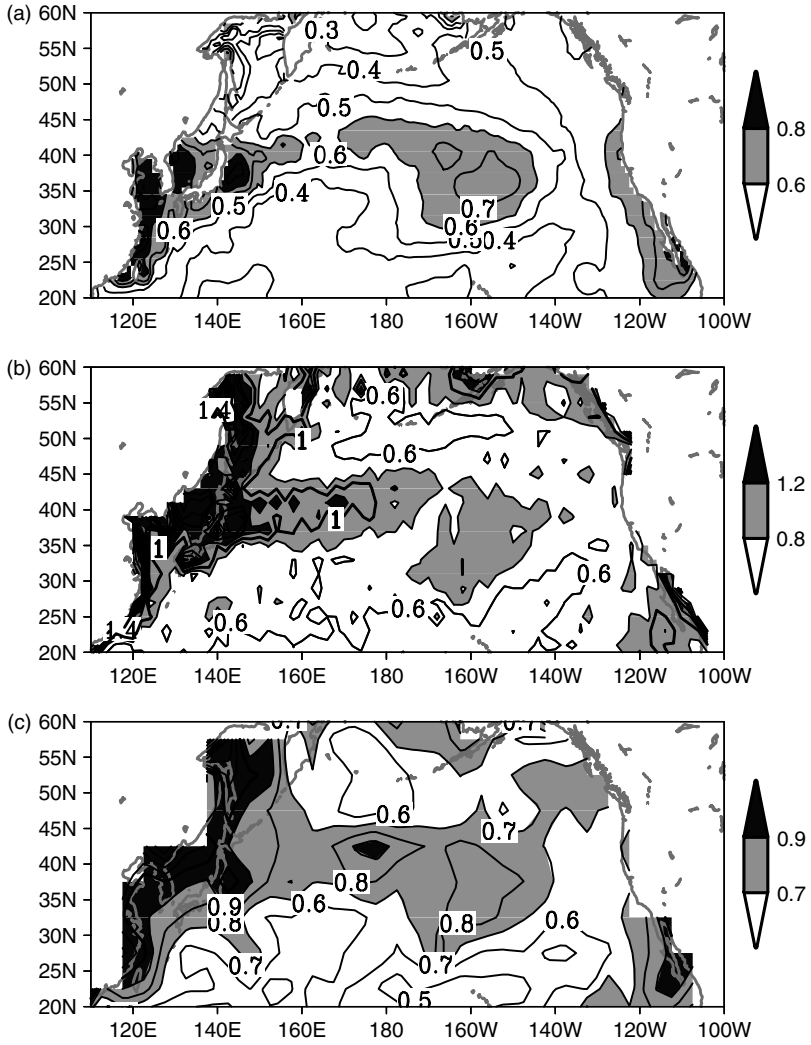

Figure 9. A Figure 6, but for the North Pacific

in these SST datasets, it is difficult to see that the STF has stronger standard deviations than those to the north and to the south.

The SAF and STF are interesting in terms of decadal climate variability and climatic regime shifts in the North Pacific. A number of papers investigated the North Pacific climatic regime shift that occurred in the 1970s (e.g. Nitta and Yamada, 1989; Trenberth, 1990). Similar climatic shifts also occurred in the 1920s and 1940s (Mantua *et al*., 1997; Minobe, 1997), and the corresponding oscillatory variability in the ocean and atmosphere is called the Pacific (inter-)decadal oscillation (PDO) by Mantua *et al*. (1997). Minobe (1999, 2000) suggested that these three climatic regime shifts are marked by simultaneous phase reversals of the bi-decadal (about 20 year) oscillation and pentadecadal (50–70 year) oscillation. An interesting feature of the 1970s regime shift is that the SST difference before and after the shift has two action centres, corresponding to the SAF and STF (Nakamura *et al*., 1997). Nakamura *et al*. (1997) suggested that the SAF variability is not related to the tropical changes, but that the STF has a close linkage with the tropics. Therefore, it is an interesting question as to what occurred for the SAF and STF associated with the 1920s and 1940s regime shifts. However, the available grids are sparse over the North Pacific at the beginning of the 20th century, and hence we focus our attention on the 1940s regime shift.

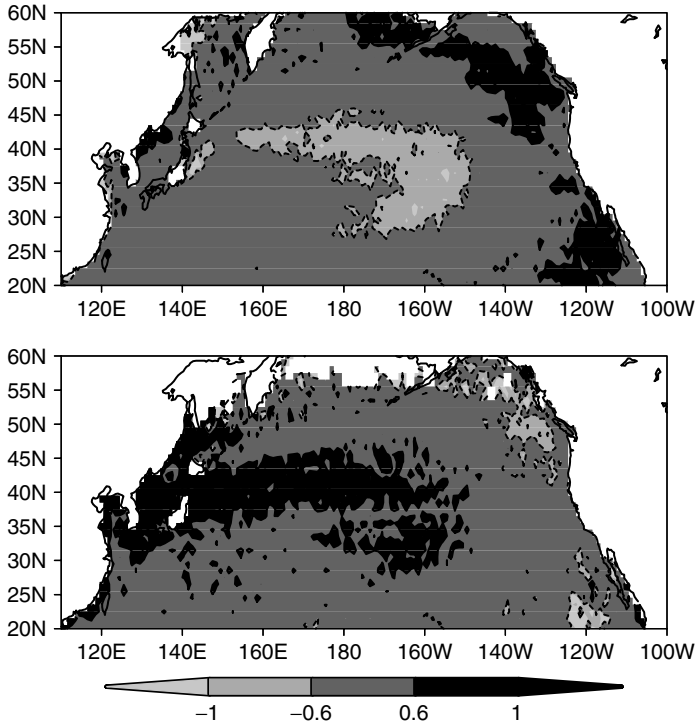

Figure 10. Winter–spring SST anomaly differences between successive two epochs of a regime associated with the 1970s (top panels) and 1940s (bottom panels) climatic regime shifts. The SST difference is calculated between 1977–97 and 1948–76 for the upper panel, and 1948–76 minus 1925–47 for the lower panel. Contours indicate ±0.6 °C

Figure 10 shows the winter–spring (December–May) SST difference between two successive epochs separated by the regime shifts in the 1970s and 1940s. The SST difference for the 1970s regime shift is consistent with the pronounced cooling centred in the SAF (around 40°N) and STF (around 33°N) as documented by Nakamura *et al*. (1997). Also, the SST changes for the 1940s regime shift exhibit the two action centres associated with the SAF and STF, though the STF change is weaker than the SAF change. The SST difference for the 1940s shift has larger amplitudes in the SAF, especially around Japan, consistent with SST analysis over the Pacific Ocean by Deser *et al*. (2004) and air-temperature analysis in Japan by Yamamoto *et al*. (1986).

A similar SST difference map was also calculated using $2^\circ \times 2^\circ$ ICOADS data (not shown). The signatures of SST warming appeared as less-prominently trapped by the SAF and STF in the ICOADS SSTs than the present SSTs, partly due to the vestiges of unrealistic grids over the central North Pacific shown in Figure 1.

Figure 11 shows the time series of the SAF and STF since 1915; before 1915, the number of observations are likely to be too small to determine the SST anomalies of the SAF and STF confidently. Also, from 1942 to 1948, the number of observations was quite small, which is associated with World War II. However, warming in the SAF and STF is prominent between two epochs: 1915–1941 and 1949–1976. Therefore, combined with Figure 10, the present result indicates that both the SAF and STF warmed associated with the 1940s regime shift. Owing to the small number observations during World War II, it is difficult to determine whether the apparent different timing of the SAF and STF warming is real or not. Although previous studies suggested that another climatic regime shift occurred in the mid 1920s in opposing polarity to the 1940s shift (Mantua *et al*., 1997; Minobe, 1997), the SAF and STF time series do not show a prominent signature in the 1920s.

The STF exhibited a rapid warming in 1999, consistent with basin-wide 1998–99 changes (Minobe, 2002). On the other hand, the SAF returned roughly to its pre-1977 condition around 1990, and did not show substantial change in 1998–99. The nature of the 1998–99 change is under debate; a key question is whether

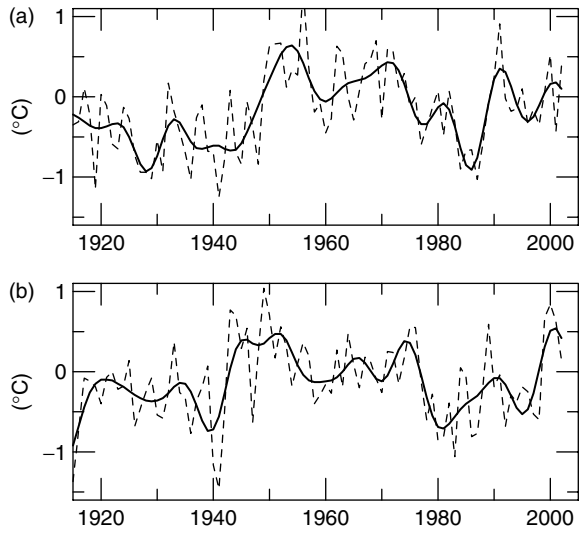

Figure 11. Time series of SST anomalies (a) for SAF (36–44 °N, 140 °E–175 °W) and (b) for STF (28–35 °N, 180–160 °W). Dashed lines denote raw anomalies, and solid curves indicate 7 year low-pass filtered data

this is another regime shift or not (e.g. Chavez *et al*., 2003). Minobe (2002) noted that the 1998–99 change is associated with the east Pacific pattern, characterized by a meridional dipole SLP over the eastern North Pacific, whereas the other three shifts, in the 1920s, 1940s and 1970s, are more closely related to strength changes in the Aleutian low. Consistently, Bond *et al*. (2003) showed that the 1998–99 change is associated with the SST second EOF mode in the North Pacific, but the 1970s shift is related to the first mode.

6. SUMMARY AND DISCUSSION

A gridded dataset of SST anomalies on a monthly $1^\circ \times 1^\circ$ grid is produced using SST observations collected in ICOADS release 2.1 without spatial interpolation and spatial smoothing. Unrealistic observations, which influenced the gridded data of ICOADS, were removed subjectively. As an application of the present SST dataset, the GSE in the North Atlantic and the SAF and STF in the North Pacific are examined.

The strong variability associated with the GSE in the winter–spring SSTs is more apparent in the present dataset than in the other widely used SST datasets, i.e. HadISST, ICOADS, and MOHSST. The GSE mean SST indicates multidecadal variability, and GSE is the strongest part of the AMO.

In the North Pacific, strong SST variability is observed over the SAF, with secondary amplitudes in the STF. Just to the east of Japan, the KE (35 °N) and OF (40 °N) marked two cores of variability. The SAF and STF were the action centres of the SST warming associated with the climatic regime shift in the 1940s, as well as the cooling in the 1970s shift, consistent with the study by Nakamura *et al*. (1997) for the 1970s shift. However, the SST change associated with the 1940s shift exhibits broader changes around the SAF than the 1970s shift and were centred in the region of Japan, consistent with the strong warming signal in air temperatures in Japan (Yamamoto *et al*., 1986).

Although we focused on the North Pacific, recent studies have shown that Pacific decadal variability and two regime shifts in the 1940s and 1970s involve the Southern Hemisphere. Zhang *et al*. (1997) and Garreaud and Battisti (1999) showed that El Niño–southern oscillation (ENSO)-like decadal variability, which is closely associated with the PDO (Mantua *et al*., 1997), has a meridionally symmetric pattern with respect to the equator. Consistently, Folland *et al*. (1999, 2002) reported that the time series for a meridionally symmetric pattern, called the interdecadal Pacific oscillation (IPO), highly resembles the PDO index. The IPO is obtained as a third EOF of low-pass filtered (period >13 years) global SSTs. Also, Linsley *et al*. (2004) showed that the IPO was well captured by South Pacific coral since 1880, though coral records seem to exhibit weaker

multidecadal variability than those found in the IPO and PDO. Thus, the decadal SAF and STF variability may be viewed as a regional manifestation of pan-Pacific decadal variability. It seems equally conceivable that the frontal variability plays an active role in the atmospheric variability (e.g. Nakamura *et al*., 1997; Tanimoto *et al*., 2003). For a better understanding of the roles of the oceanic fronts, further investigations are necessary.

No spatial interpolation or spatial smoothing in the present SST dataset ensures a high effective spatial resolution, but inevitably results in a noisy monthly SST field. Thus, it may not be a good idea to show an SST snapshot at a certain month using these data. However, when we want to know the detailed spatial structures of averaged values (e.g. long-term means or GSE mean) or statistics (e.g. standard deviation), the present dataset can provide useful information that cannot be adequately obtained in other SST datasets.

ACKNOWLEDGEMENTS

We thank to Dr Woodruff and Ms Manabe for encouraging us to submit this paper, and Dr Folland and an anonymous reviewer for their fruitful comments. This study was supported by grant-in-aid for scientific research (kaken-hi no 15540417) and by 21st century Center of Excellence program on 'Neo-Science of Natural History' (leader Professor H. Okada) both from the Ministry of Education, Culture, Sports, Science and Technology, Japan.

REFERENCES

Bond NA, Overland JE, Spillane M, Stabeno P. 2003. Recent shifts in the state of the North Pacific. *Geophysical Research Letters* **30**: 2183. DOI: 10.1029/2003GL018597.

Chavez FP, Ryan J, Lluch-Cota SE, Niquen CM. 2003. From anchovies to sardines and back: multidecadal change in the Pacific Ocean. *Science* **299**: 217–221.

Deser C, Blackmon ML. 1993. Surface climate variations over the North Atlantic Ocean during winter: 1900–1989 *Journal of Climate* **6**: 1743–1753.

Deser C, Phillips AS, Hurrell JW. 2004. Pacific interdecadal climate variability: linkages between the tropics and North Pacific during boreal winter since 1900. *Journal of Climate* **17**: 3109–3124.

Enfield DB, Mestas-Nuñez AM, Timble PJ. 2001. The Atlantic multidecadal oscillation and its relation to rainfall and river flows in the continental U.S. *Geophysical Research Letters* **28**: 2077–2080.

Folland CK, Parker DE. 1995. Correction of instrumental biases in historical sea surface temperature data. *Quarterly Journal of the Royal Meteorological Society* **121**: 319–367.

Folland CK, Parker DE, Palmer TN. 1986. Sahel rainfall and worldwide sea temperatures 1901–85. *Nature* **320**: 602–607.

Folland CK, Parker DE, Colman A, Washington R. 1999. Large scale modes of ocean surface temperature since the late nineteenth century. In *Beyond El Nino: Decadal and Interdecadal Climate Variability*, Navarra A (ed.). Springer-Verlag: Berlin; 73–102.

Folland CK, Renwick JA, Salinger MJ, Mullan AB. 2002. Relative influences of the interdecadal pacific oscillation and ENSO on the South Pacific convergence zone. *Geophysical Research Letters* **29**: DOI: 10.1029/2001GL014201.

Frankignoul C, Coëtlogon GD, Joyce TM, Dong S. 2001. Gulf Stream variability and ocean–atmosphere interaction. *Journal of Climate* **31**: 3516–3529.

Garreaud RD, Battisti DS. 1999. Interannual (ENSO) and interdecadal (ENSO-like) variability in the Southern Hemisphere tropospheric circulation. *Journal of Climate* **12**: 2113–2123.

Ishii M, Shouji A, Sugimoto S, Matsumoto T. 2005. Objective analyses of sea-surface temperature and marine meteorological variables for the 20th century using ICOADS and the Kobe Collection. *International Journal of Climatology* **25**: 865–879; this issue.

Joyce TM, Deser C, Spall MA. 2000. The relation between decadal variability of subtropical mode water and the North Atlantic oscillation. *Journal of Climate* **13**: 2550–2569.

Kaplan A, Kushnir Y, Cane M, Blumenthal B. 1997. Reduced space optimal analysis for historical datasets: 136 yrs of Atlantic sea surface temperatures. *Journal of Geophysical Research* **102**: 27 835–27 860.

Linsley BK, Wellington GM, Schrag DP, Ren L, Salinger M, Tudhope AW. 2004. Geochemical evidence from corals for changes in the amplitude and spatial pattern of South Pacific interdecadal climate variability over the last 300 years. *Climate Dynamics* **22**: 1–11.

Manabe T. 1999. The digitized Kobe Collection phase I: historical surface marine meteorological observations in the archive of the Japan Meteorological Agency. *Bulletin of the American Meteorological Society* **80**: 2703–2715.

Mantua NJ, Hare SR, Zhang Y, Wallace JM, Francis RC. 1997. A Pacific interdecadal climate oscillation with impacts of salmon production. *Bulletin of the American Meteorological Society* **78**: 1069–1079.

Minobe S. 1997. A 50–70 year climatic oscillation over the North Pacific and North America. *Geophysical Research Letters* **24**: 683–686.

Minobe S. 1999. Resonance in bidecadal and pentadecadal climate oscillations over the North Pacific: role in climatic regime shifts. *Geophysical Research Letters* **26**: 855–858.

Minobe S. 2000. Spatio-temporal structure of the pentadecadal variability over the North Pacific. *Progress in Oceanography* **47**: 381–408.

Minobe S. 2002. Interannual to interdecadal changes in the Bering Sea and concurrent 1998/99 changes over the North Pacific. *Progress in Oceanography* **55**: 45–64.

Mizuno K, White WB. 1983. Annual and interannual variability in the Kuroshio Current system. *Journal of Physical Oceanography* **13**: 1847–1867.
Nakamura H, Lin G, Yamagata T. 1997. Decadal climate variability in the North Pacific during the recent decades. *Bulletin of the American Meteorological Society* **98**: 2215–2225.
Nitta T, Yamada S. 1989. Recent warming of tropical sea surface temperature and its relationship to the Northern Hemisphere circulation. *Journal of the Meteorological Society of Japan* **67**: 375–383.
Palmer T, Sun Z. 1985. A modeling and observational study of the relationship between sea surface temperature in the north west Atlantic and atmospheric general circulation. *Quarterly Journal of the Royal Meteorological Society* **111**: 947–975.
Parker DE, Folland CK, Jackson M. 1995. Marine surface temperature: observed variations and data requirements. *Climatic Change* **31**: 559–600.
Ratcliffe RAS, Murray R. 1970. New lag associations between North Atlantic sea temperatures and European pressure, applied to long-range weather forecasting. *Quarterly Journal of the Royal Meteorological Society* **96**: 226–246.
Rayner NA, Parker DE, Horton EB, Folland CK, Alexander LV, Rowell DP, Kent EC, Kaplan A. 2003. Global analyses of sea surface temperature, sea ice, and night marine air temperature since the late nineteenth century. *Journal of Geophysical Research* **108**(D14): 4407. DOI: 10.1029/2002JD002670.
Reynolds RW, Smith TM. 1994. Improved global sea-surface temperature analyses using optimum interpolation. *Journal of Climate* **7**: 929–948.
Schneider N, Miller AJ, Pierce DW. 2002. Anatomy of North Pacific decadal variability. *Journal of Climate* **15**: 586–605.
Seager R, Kushnir Y, Naik NH, Cane MA, Miller J. 2001. Wind-driven shifts in the latitude of the Kuroshio–Oyashio extension and generation of SST anomalies on decadal timescales. *Journal of Climate* **14**: 4249–4265.
Smith TM, Reynolds RW. 2004. Improved extended reconstruction of SST (1854–1997). *Journal of Climate* **17**: 2466–2477.
Tanimoto Y, Nakamura H, Kagimoto T, Yamane S. 2003. An active role of extratropical sea surface temperature anomalies in determining anomalous turbulent heat flux. *Journal of Geophysical Research* **108**(C10): 3304. DOI: 10.1029/2002JC001750.
Trenberth KE. 1990. Recent observed interdecadal climate changes in the Northern Hemisphere. *Bulletin of the American Meteorological Society* **71**: 988–993.
Woodruff SD, Slutz RJ, Jenne RL, Steurer PM. 1987. A comprehensive ocean–atmosphere data set. *Bulletin of the American Meteorological Society* **68**: 1239–1250.
Worley SJ, Woodruff SD, Reynolds RW, Lubker SJ, Lott N. 2005. ICOADS release 2.1 data and products. *International Journal of Climatology* **25**: 823–842; this issue.
Wu P, Rodwell M. 2003. Gulf Stream forcing of the winter North Atlantic oscillation. *Atmospheric Science Letters* **5**: 57–64. DOI: 10.1016/j.atmoscilet.2003.12.002.
Yamamoto R, Iwashima T, Sanga NK, Hoshiai M. 1986. An analysis of climate jump. *Journal of Meteorological Society of Japan* **64**: 273–281.
Zhang Y, Wallace JM, Battisti DS. 1997. ENSO-like interdecadal variability: 1900–1993. *Journal of Climate* **10**: 1004–1020.

